

© 2021 IEEE. Personal use of this material is permitted. Permission from IEEE must be obtained for all other uses, in any current or future media, including reprinting/republishing this material for advertising or promotional purposes, creating new collective works, for resale or redistribution to servers or lists, or reuse of any copyrighted component of this work in other works.

# Electromagnetic Fields on 3-Phase Induction Motor Using Finite Element Analysis

1<sup>st</sup> Douglas Nascimento\*  
University of Zielona Góra  
University of Twente  
Zielona Góra, Poland  
eng.douglas.a@ieee.org

2<sup>nd</sup> Robert Smolenski  
Instytut Automatyki,  
Elektroniki i Elektrotechniki  
University of Zielona Góra  
Zielona Góra, Poland  
r.smolenski@iee.uz.zgora.pl

3<sup>rd</sup> Hermes Loschi  
University of Zielona Góra  
University of Twente  
University of Nottingham  
Zielona Góra, Poland  
eng.hermes.loschi@ieee.org

4<sup>th</sup> Flavia Grassi  
Dipartimento di Elettronica,  
Informazione e Bioingegneria  
Politecnico di Milano  
Milano, Italy  
flavia.grassi@polimi.it

5<sup>th</sup> Lu Wan  
Dipartimento di Elettronica,  
Informazione e Bioingegneria  
Politecnico di Milano  
Milano, Italy  
lu.wan@polimi.it

6<sup>th</sup> Abduselam Hamid  
Dipartimento di Elettronica,  
Informazione e Bioingegneria  
Politecnico di Milano  
Milano, Italy  
abduselamhamid.beshir@polimi.it

**Abstract**—Electromagnetic fields of a 3-phase induction motor, i.e., electric and magnetic fields and current density, are highly influenced by its geometry, conductor material (conductivity, magnetic permeability, electric permittivity, and nonlinearity), and boundary conditions applied (interface between conductors and dielectrics). Through Finite Element Analysis (FEA), the behavior of electromagnetic fields can be predicted. Thus, favoring the electromagnetic interference mitigation techniques of the 3-phase induction motor. Therefore, this paper presents numerical modeling with FEA, based on COMSOL, as an early pre-compliance tool to investigate the current density distribution and electric and magnetic fields. The validation of the modeling approach will be presented and discussed considering a 3-phase induction motor. Furthermore, CISPR 25 will be considered to evaluate the interactions between electric and magnetic fields, current density distribution, and skin effect on an increasing frequency.

**Index Terms**—Finite Element Analysis, Electromagnetic Interference, 3-Phase Induction Motor, Electromagnetic Fields.

## I. INTRODUCTION

Nowadays, with the growing demand for sustainable adoption of battery electric vehicles (BEV), 3-phase induction motors have been used in various applications, including vehicular power and propulsion systems and electrified powertrains [1]. The 3-phase induction motor (IM) modeling approaches in higher frequencies (upper fundamental frequency) are discriminated into: behavioral and numerical modeling. Numerical modeling creates equivalent circuits of the 3-phase IM using 3-D electromagnetic (EM) field analysis (provided by software). In contrast, behavioral modeling provides equivalent circuits


representation through measurement data at the 3-phase IM output ports (e.g., using hardware setup) [1], [2].

One type of numerical modeling for EM fields simulation is the Finite Element Analysis (FEA), a well diffused technique through several science subjects. A reason behind it can be attributed to the capability to tackle complex geometries, since FEA uses unstructured grid meshing in the geometry. Thus, FEA tools need to have the full volume meshing of the equipment under test (EUT) [3]. Some papers address 3-phase IM numerical simulation using FEA, however, they are not very detailed in terms of the volume meshing definition and materials specification [4]–[7].

In addition, since the 3-phase IM might generate electromagnetic interference (EMI) through radiated or conducted emission, affecting the surrounding electromagnetic environment [8]. Several normative requirements are applied to systems infrastructure which consider 3-phase IM, e.g., BEV. CISPR 36 [9], CISPR25 [10], CISPR 12 [11], IEC 61000-6-3 [12] are applied for stand-alone devices (and components) and to the entire fully equipped vehicle [13], [14].

Therefore, once the volume meshing definition and materials specification are fundamental parameters to provide a proper FEA, establishing the EM fields boundary conditions. This paper presents numerical modeling with FEA, based on COMSOL, as an early pre-compliance tool to investigate the current density distribution and electric and magnetic fields. Thus, this approach creating numerical modeling with FEA might be expanded for all types of electric motors. Moreover, in this paper, the modeling approach's validation will be presented and discussed considering a 3-phase IM. Furthermore, the CISPR 25 will be considered as the frequency range of analysis.

Nonetheless, the main contribution of current paper resides

This paper has received funding from the European Union's Horizon 2020 research and innovation programme under the Marie Skłodowska-Curie grant agreement No.812753 and No.812391. 

\*Corresponding author: eng.douglas.a@ieee.org (Douglas Nascimento).

in the description and details of the materials and constructive aspects used in the motor and comparison of the data obtained with the literature. The results here presented can, therefore, serve as a reference for further comparison in either simulated or experimental environment.

The paper is addressed as follows. In the second Section, the overview of IM applications for electric vehicles is described, as well as the FEA approach in terms of mathematical approach regarding the Maxwell equations. In the third Section, details on the FEA as an EM fields simulation tool are presented. In the fourth Section, the 3-phase IM's EM fields levels are gathered from the software simulation, and the data results are discussed. Also, some comparisons with other studies about the levels of EM fields are performed. Finally, the conclusion is addressed in the fifth Section, as well as the future studies.

## II. 3-PHASE INDUCTION MOTOR FOR ELECTRIC VEHICLES

The most common electric motors available in the market are mainly classified based on the input types as alternating current (AC) motors and direct current (DC) motors as shown in Fig. 1. However, in the BEV industry, the IM types have become the most favored ones with the advanced development of their power electronic systems due to the efficient reliability [15].

The EM fields analysis is essential to ensure the machinery lifespan once instantaneous voltage summation in the 3-phase coils of an IM (common mode voltage) is not zero. In addition, those effects yield high-frequency (HF) leakage current, which leads to EMC issues. As result it can cause shaft voltage, bearing current, stator winding overvoltage and turn-to-turn voltage stress which drastically reduces the equipment lifespan [16]. Therefore, identifying the EMI footprint at high frequencies is mandatory as the first step leading to mitigation actions afterward.

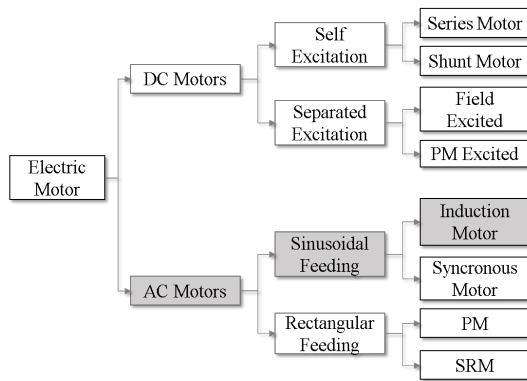


Fig. 1. Common types of electric motors for electric vehicles, based on [17], [18].

### A. High Frequency Modeling of AC Rotary Machine

There are two types of EMI coupling traditionally considered in the HF modeling due to the crosstalk phenomena:

capacitive and inductive coupling. The capacitive coupling results from the electric field interactions caused by the stray capacitance between two or more conductors. However, the inductive coupling is induced by the influence of the magnetic field between circuits [3], [19]. For the present study, once the upper frequency range of analysis is restricted to 300 kHz, the stray capacitance will be neglected, focusing on the skin depth and current displacement of the frequency.

For the parasitic inductance and metal materials, the skin effect will play a major role in the current density distribution. In the fundamental frequency, the higher current density will take place at the center of the conductor. In contrast, the lower current density is nearly uniformly distributed on the conductor's surface (boundary). Above the fundamental frequency, the current density will be progressively displaced to the conductor boundary. The skin depth ( $\delta$ ) of a metallic material is usually approximated as (1).

$$\delta = \frac{1}{\sqrt{\pi \cdot f \cdot \mu \cdot \sigma}} \quad (1)$$

where  $\sigma$  is the conductivity,  $f$  is the frequency,  $\mu$  is the absolute permeability and it is given by  $\mu = \mu_0 \mu_r$ . The  $\mu_0$  is the vacuum permeability as  $4 \cdot \pi \cdot 10^{-7} H/m$  and  $\mu_r$  is the relative permittivity (from material) of the conductor and  $\sigma$  is the conductivity [19], [20].

Therefore, the skin depth is useful to evaluate the impact of the conductor cross sectional area due to the electric and magnetic fields and the current density distribution with the increase of frequency, and also as an estimation of the conductor resistance [20].

### B. Equations Formulation for Electromagnetic Analysis

The assessment of EM fields is to solve the Maxwell's equations subject to certain boundary conditions. The differential form is presented here because it leads to differential equations that the finite element analysis can handle [21]. Thus, considering an alternating electric current over a conductor, which generates an electric field, the behavior of this phenomenon is ruled according to the general Maxwell-Ampère's law [22]:

$$\nabla \times \mathbf{H} = \mathbf{J} + \frac{\partial \mathbf{D}}{\partial t} \quad (2)$$

where  $\mathbf{H}$  is the magnetic field,  $\mathbf{J}$  is the current density and  $\mathbf{D}$  is the electric flux density. The quasi-static approximation (consideration of stationary current on each instant) implies that the equation of continuity can be written as  $\nabla \cdot \mathbf{J} = 0$  [23]. The time derivative of the electric displacement  $\partial \mathbf{D} / \partial t$  can be disregarded in Maxwell-Ampère's law [22]. Then, the general Ampère-Maxwell is rewritten into:

$$\nabla \times \mathbf{H} = \mathbf{J} \quad (3)$$

In this study, the EM fields are analyzed in the frequency domain carried out by using Magnetic Fields physics under AC/DC module from COMSOL software. Therefore, to derive

the time harmonic equation in this physics interface solver, it is used (3) including displacement currents, once it is not demanded high computational load in the frequency domain, thus:

$$\mathbf{J} + \frac{\partial \mathbf{D}}{\partial t} = \sigma \mathbf{E} + j\omega \mathbf{D} + \sigma \mathbf{v} \times \mathbf{B} + \mathbf{J}_e \quad (4)$$

where  $\mathbf{E}$  is the electric field,  $\mathbf{B}$  is the magnetic flux density and  $\mathbf{v}$  is the velocity and  $\mathbf{J}_e$  is the current density generated at external. Knowing that  $\mathbf{B} = \mu_0 \mathbf{H} + \mathbf{M}$  and  $\mathbf{D} = \epsilon_0 \mathbf{E}$ , in which  $\epsilon_0$  is the permittivity of vacuum of with value of  $8.85 \cdot 10^{-12} F/m$ , and the  $\mathbf{M}$  is the magnetization vector, the Ampère's Law can be rewritten as:

$$(j\omega\sigma - \omega^2\epsilon_0)\mathbf{A} + \nabla \times (\mu_0^{-1}\nabla \times \mathbf{A} - \mathbf{M}) - \sigma \mathbf{v} \times (\nabla \times \mathbf{A}) = \mathbf{J}_e \quad (5)$$

where  $\mathbf{V}$  is the electric scalar potential and  $\mathbf{A}$  the magnetic vector potential. Thus, it is convenient to express problems in terms of potentials, over 3D Euclidean space and time as:

$$\mathbf{B} = \nabla \times \mathbf{A} \quad (6)$$

$$\mathbf{E} = -j\omega \mathbf{A} \quad (7)$$

The equations (6) and (7) are important to obtain the current density and the electric and magnetic fields over the 3-phase IM face using FEA. In addition, for the materials specifications, all the calculation might be performed considering  $\mathbf{B} = \mu_0 \mu_r \mathbf{H}$  and  $\mathbf{D} = \epsilon_0 \epsilon_r \mathbf{E}$ . Both  $\mathbf{E}$  and  $\mathbf{D}$  are inherent regarding the motor defined materials.

### III. FINITE ELEMENT ANALYSIS AS AN EM FIELDS SIMULATION TOOL

When dealing with FEA, some steps are demanded: building the geometry, defining the models, materials and boundary conditions, meshing the structures, and analyzing results using post processing. Firstly, the domain of the object is divided into finite elements with a pre-selected shape depending on the dimension (e.g. tetrahedral, triangle, square, etc). After that, field equations are applied to the surfaces of each element in order to obtain the unknown coefficients. As the equations are gathered, their elements are organized in matrix form. Therefore, the FEM software produces sparse equation matrix, which is able to tackle the object boundaries with different materials in an efficient way [3], [24].

#### A. Simulation Model

A 3-phase squirrel-cage IM was used as a model at no load condition. The CAD model is available by the owner of the software as described in [25], and illustrated in Fig. 2.

The 3-phase IM rotor consists of an iron core and an aluminum skewed squirrel cage. The cage is made of 24 bars with a tilt of 30 degrees/m. The stator is made of 6 coils (single

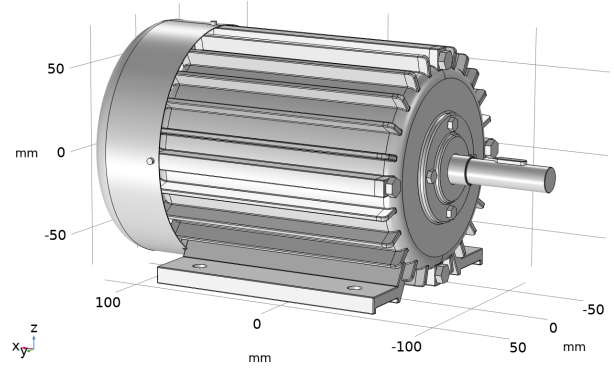


Fig. 2. 3-phase IM model.

windings) with 3 slots per pole and phase, which makes a total of 36 slots for such a 2 pole pairs design. The stator core is made of soft iron and the stator coils are made of copper. Furthermore, the materials used to define objects domains and boundaries are described in Table I.

TABLE I  
MATERIALS SPECIFICATION USED IN THE SIMULATION.

Material	Mechanic Component	$\sigma$ [S/m]	$\mu_r$	$\epsilon_r$
White Iron	Housing	$1.92 \cdot 10^6$	1200	1
Air	Air Gap	$2.5 \cdot 10^{-8}$	1	1
Cooper	Stator coils	$5.998 \cdot 10^7$	1	1
Laminated steel	Shaft, cores	$2.17 \cdot 10^8$	4000	1
Aluminum	Rotor coils	$3.774 \cdot 10^7$	1	1

In order to establish the FEA, the following currents to the coils were considered:  $I_1 = 5\sqrt{2} \cdot \exp(j2\pi)A$  (coil A),  $I_2 = 5\sqrt{2} \cdot \exp(j2\pi/6)A$  (coil B) and  $I_3 = 5\sqrt{2} \cdot \exp(j2\pi/3)A$  (coil C), for the supply frequency of 50 Hz. The  $I_1$ ,  $I_2$ , and  $I_3$  are phasors defined by the rms of peaks of the corresponding sinusoid.

#### B. Meshing and Boundary Conditions

In this study, the 2D simulation is defined over the 3-phase IM transverse cross-section. The model meshing is shown in Fig. 3. In order to cover the minor parts of the 3-phase IM, it was chosen extra-fine element size, which provides a suitable refinement for complex structures. Then, the EM fields could be obtained.

## IV. RESULTS AND DISCUSSION

Aiming to understand the EM fields behavior, the simulations were performed to extract current density and electric and magnetic fields for different frequency conditions to assess the 3-phase IM performance. The frequencies defined are 50 Hz, 10 kHz, 100 kHz, and 300 kHz, following CISPR 25.

#### A. Current Density and Skin Effect

The current density distribution obtained for the upper and lower frequencies, i.e., 50 Hz and 300 kHz, is shown in Fig. 4 and Fig. 5, respectively.

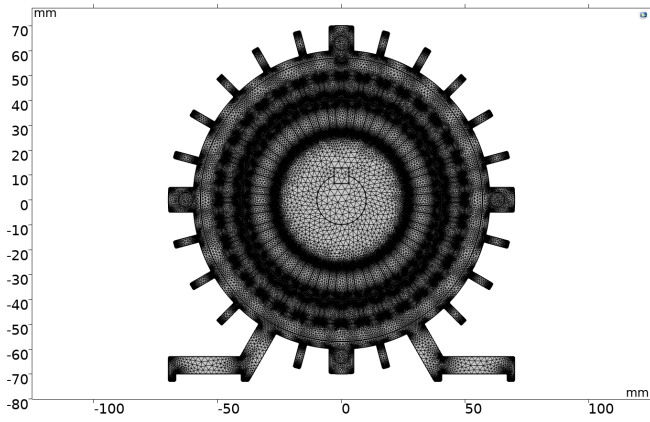


Fig. 3. Model meshing on the 3-phase IM transverse cross section workplane.

As presented in the Fig. 4 and Fig. 5, in all the frequencies (50 Hz, 10 kHz, 100 kHz, and 300 kHz), the analysis took into account measurements using probe over the normal vector (outward on the y-z plan surface) of the parameters by the 3-phase IM axial cross section in -70 to 70 mm x-axis and centralized in origin for y-axis - using a cut line 2D tool in the software (sweeping measurement). Likewise, the x-axis graph interval (Figures 6, 7, 8 and 9) considers the longitudinal symmetric distribution, however, from 0 to 140 m to present the field probe values instead due to using arc length (length interval for display data).

Considering the arc length (cut line) over the 3-phase IM face workplane, Fig. 6 compares the current density for each analyzed frequency. It is noted that the current density profile is longitudinal symmetric along the x-axis, from left to right (0-70 mm): the first (outer) peak occurs nearby the stator, followed by the second peak in the air gap between the stator and rotor and the third (inner) surge appears at the edges of rotor coil. The rotor core has no current changing ( $dI/dt = 0$ ) so the current density at the middle of the chart is null. The same explanation is reciprocal from 70 to 140 mm.

In addition, Fig. 6 shows that for 10 kHz and above, the

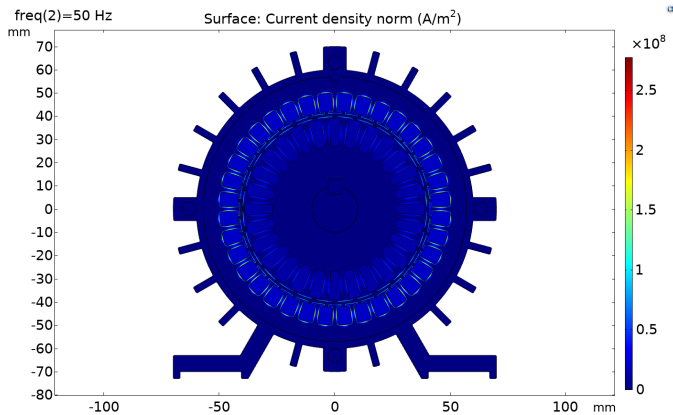


Fig. 4. Current density over the 3-phase IM transverse cross section at 50 Hz.

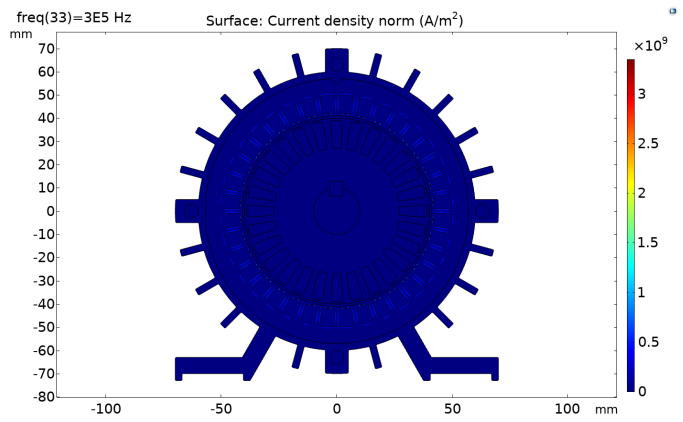


Fig. 5. Current density over the 3-phase IM transverse cross section at 300 kHz.

profile changes completely from approximately  $4.5 \cdot 10^7 A/m^2$  (in the rotor's coil, at 50 Hz) and it is shifted to the 3-phase IM housing where it reaches  $6 \cdot 10^7 A/m^2$  as a result of the skin effect.

### B. Electric and Magnetic Fields

The electric field profile is shown in Fig. 7. Basically it exhibits a similar distribution as the current density (Fig. 6) where it varies from 0.45 V/m (between the stator and the rotor) at 50 Hz into 0.3 V/m for 10 kHz. In the frequencies of 100 kHz to 300 kHz, the currents density distribution has practically the same behavior, with peaks just above 0.25 V/m.

The magnetic field, however, shows a different demeanor. Fig. 8 shows that at 50 Hz, the value of magnetic field strength in the rotor's coil is about  $2.8 \cdot 10^5 A/m$  and this value is too intense compared to the other boundaries (for this reason, only two peaks are visible in the plot).

In the case of the frequency equal to 300 kHz, as illustrated in Fig. 9, it is possible to observe that the intensity of the magnetic field achieves around  $0.9 A/m$  and it has two peaks, resulting in the current displacement to the surrounding stator's coil and the air gap.

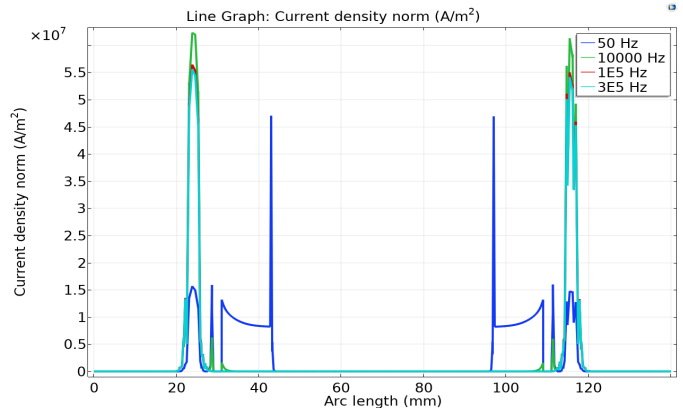


Fig. 6. Current density over the cut line in the 3-phase IM transverse cross section for 50 Hz, 10 kHz, 100 kHz and 300 kHz.

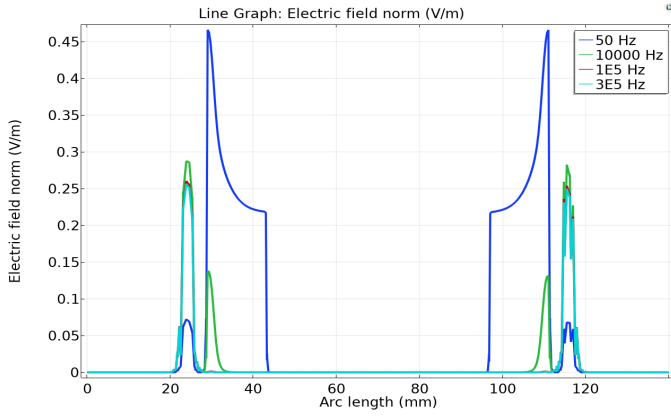


Fig. 7. Electric field at 50 Hz, 10 kHz, 100 kHz and 300 kHz.

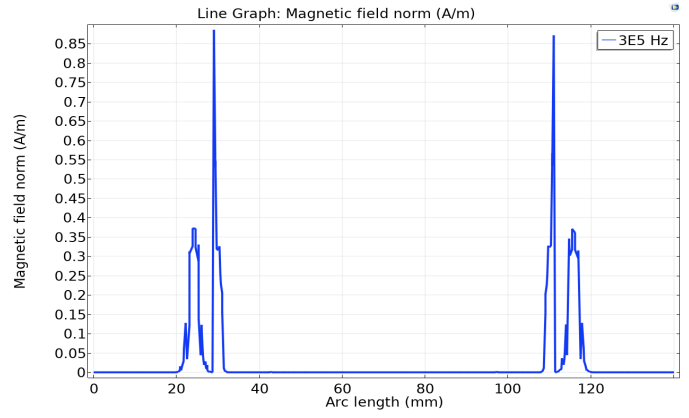


Fig. 9. Magnetic field at 300 kHz.

### C. Comparison with other Studies

The results showed in Table II demonstrates that the values found are consistent (same order of magnitude) with those found in previous works available in [26]–[28].

TABLE II  
CURRENT DENSITY COMPARISON BETWEEN THE THIS PAPER AND REFERENCES.

	Frequency (Hz)	Current Density (A/m <sup>2</sup> )
This paper.	50	4.704e+7
	10e+3	6.233e+7
	300e+3	5.561e+7
[26]	50	3e+7
[27]	10e+3	1.8e+8
[28]	50	8e+7

On one hand, the proximity in order of magnitude presented in Table II, is primarily due to the definition of the copper material to be used in the stator coils instead of aluminum (see in Table I). Thus, improving the IM performance provides a better concatenating of the EM fields [29]. On another hand, the deviation in the values can be attributed to the changing between the field probe placements and also to the material used in rotor and stator.

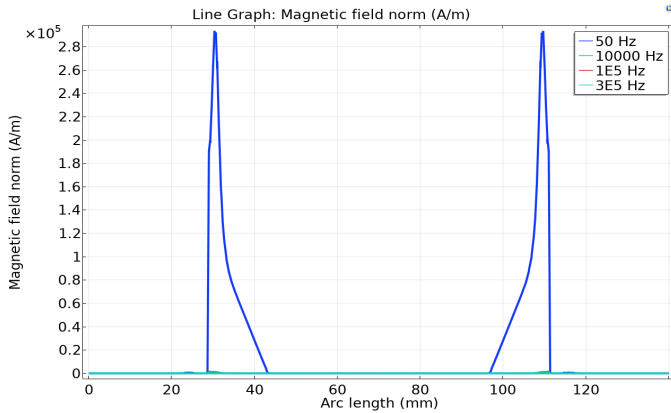


Fig. 8. Magnetic field at 50 Hz, 10 kHz, 100 kHz and 300 kHz.

### V. CONCLUSION

This paper presented numerical modeling with FEA, based on COMSOL. Considering the 3-phase IM model, the EM fields, i.e., current density, electric and magnetic fields, were analyzed in the frequencies of 50 kHz, 10 kHz, 100 kHz, and 300 kHz as specified in the normative CISPR 25. It was found that the behavior of those parameters significantly changes with frequency, mainly due to the current displacement induced by the skin effect, boundary conditions, the frequency response of the IM, and the secondary effects (i.e., non-linearity of the materials applied voltage, etc.).

The results comparison presented in table II, raise the hypothesis that the existing 3-phase IM model perhaps could also be used in BEV applications. On the one hand, that hypothesis reinforces and validates FEA's proposed modeling approach, based on COMSOL. However, on the other hand, a more detailed study considering copper as the coil material, the efficiency and losses computing of the IM performance is still necessary, as well as consider the traditional geometry of IM applicable to BEV.

Thus, it is intended to analyze the efficiency and losses of a 3-phase IM model for both no-load and specific loading conditions considering both conducted and radiated emissions for future studies. Also, new materials arranging and the stray elements (either capacitance and inductance) will be taken into account.

### ACKNOWLEDGMENT

The authors would like to thanks the Institute of Automatic Control, Electronics, and Electrical Engineering at the University of Zielona Góra and the Dipartimento di Elettronica, Informazione e Bioingegneria of the Politecnico di Milano for the facilities and equipments for carrying out the simulations and studies.

### REFERENCES

- [1] B. Bilgin, J. Liang, M. V. Terzic, J. Dong, R. Rodriguez, E. Trickett, and A. Emadi, "Modeling and Analysis of Electric Motors: State-of-the-Art Review," *IEEE Transactions on Transportation Electrification*, vol. 5, no. 3, pp. 602–617, 2019.

- [2] I. Stevanovic, B. Wunsch, and S. Skibin, "Behavioral high-frequency modeling of electrical motors," *Conference Proceedings - IEEE Applied Power Electronics Conference and Exposition - APEC*, no. 4, pp. 2547–2550, 2013.
- [3] S. Alexandersson, "Automotive Electromagnetic Compatibility: Prediction and Analysis of Parasitic Components in Conductor Layouts," Ph.D. dissertation, Lund University, 2008.
- [4] L. Roubache, K. Boughrara, and R. Ibtouen, "Analytical electromagnetic analysis of multi-phases cage rotor induction motors in healthy, broken bars and open phases conditions," *Progress In Electromagnetics Research B*, vol. 70, no. 1, pp. 113–130, 2016.
- [5] W. Zaabi, Y. Bensalem, and H. Trabelsi, "Analysis of Induction Motor with Stator Winding Short-circuit Fault by Finite Element Model," vol. 3, no. 3, pp. 53–58, 2015.
- [6] N. Minh, K. Master, and S. T. Stockholm, "Predicting Electromagnetic Noise in Induction Motors," p. 73, 2014.
- [7] M. A. Iqbal and V. Agarwal, "Investigation & Analysis of Three Phase Induction Motor Using Finite Element Method for Power Quality," vol. 7, no. 9, pp. 901–908, 2014.
- [8] J. Hu, X. Xu, D. Cao, and G. Liu, "Analysis and optimization of electromagnetic compatibility for electric vehicles," *IEEE Electromagnetic Compatibility Magazine*, vol. 8, no. 4, pp. 50–55, 2019.
- [9] IEC, "CISPR 36 – Electric and hybrid electric road vehicles – Radio disturbance characteristics – Limits and methods of measurement for the protection of off-board receivers below 30 MHz," Tech. Rep., 2020.
- [10] —, "CISPR 25 – Vehicles, boats and internal combustion engines – Radio disturbance characteristics – Limits and methods of measurement for the protection of on-board receivers," Tech. Rep., 2016.
- [11] —, "CISPR 12 – Vehicles, boats and internal combustion engines – Radio disturbance characteristics – Limits and methods of measurement for the protection of off-board receivers," Tech. Rep., 2009.
- [12] —, "IEC 61000 – Electromagnetic compatibility (EMC)– Part 6-3: Generic standards – Emission standard for equipment in residential environments," Tech. Rep., 2020.
- [13] D. Das, A. Elfrgani, and C. J. Reddy, "Simulation of Conductive and Radiated Emission for off and On-Board Radio Receivers according to CISPR 12 and 25," *SAE Technical Papers*, vol. 2020-April, no. April, pp. 1–6, 2020.
- [14] F. Un-Noor, S. Padmanaban, L. Mihet-Popa, M. N. Mollah, and E. Hosain, "A comprehensive study of key electric vehicle (EV) components, technologies, challenges, impacts, and future direction of development," *Energies*, vol. 10, no. 8, pp. 1–82, 2017.
- [15] A. Karki, S. Phuyal, D. Tuladhar, S. Basnet, and B. P. Shrestha, "Status of pure electric vehicle power train technology and future prospects," *Applied System Innovation*, vol. 3, no. 3, pp. 1–28, 2020.
- [16] K. Maki, H. Funato, and L. Shao, "Motor modeling for EMC simulation by 3-D electromagnetic field analysis," *2009 IEEE International Electric Machines and Drives Conference, IEMDC '09*, pp. 103–108, 2009.
- [17] D. U. Thakar and R. A. Patel, "Comparison of Advance and Conventional Motors for Electric Vehicle Application," *2019 3rd International Conference on Recent Developments in Control, Automation and Power Engineering, RDCAPE 2019*, pp. 137–142, 2019.
- [18] Y. A. Alamoudi, A. Ferrah, R. Panduranga, A. Althobaiti, and F. Mulolani, "State-of-the Art Electrical Machines for Modern Electric Vehicles," *2019 Advances in Science and Engineering Technology International Conferences, ASET 2019*, pp. 1–8, 2019.
- [19] E. M. Montrose M. I. Nakauchi, *Testing for EMC Compliance: Approaches and Techniques*, 2004.
- [20] S. Madsen and C. Mieritz, "Current Distribution and Magnetic Fields in Complex Structures Using Comsol Multiphysics," *Comsol.Com*, 2011. [Online]. Available: <http://www.comsol.com/papers/10873/>
- [21] S. Koch, H. Schneider, and T. Weiland, "A low-frequency approximation to the maxwell equations simultaneously considering inductive and capacitive phenomena," *IEEE Transactions on Magnetics*, vol. 48, no. 2, pp. 511–514, 2012.
- [22] M. N. O. Sadiku, *Elements of Electromagnetics*. Oxford University Press Inc, 2011.
- [23] COMSOL, "AC\DC Module: User's Guide," Tech. Rep., 2018.
- [24] A. C. Cangellaris, "Frequency-Domain Finite Element Methods for Electromagnetic Field Simulation: Fundamentals, State of the Art, and Applications to EMI/EMC Analysis," in *Proceedings of Symposium on Electromagnetic Compatibility*, 1996, pp. 107–116.
- [25] COMSOL, "Two-Pole Three-Phase Induction Motor," Tech. Rep., 2017.
- [26] E. Sulaiman, M. Z. Ahmad, T. Kosaka, and N. Matsui, "Design optimization studies on high torque and high power density hybrid excitation flux switching motor for HEV," *Procedia Engineering*, vol. 53, no. 1, pp. 312–322, 2013.
- [27] N. Boucenna, S. Hlioui, B. Revol, and F. Costa, "A detailed analysis of the propagation paths of high-frequency common mode currents in AC motors," *2013 15th European Conference on Power Electronics and Applications, EPE 2013*, 2013.
- [28] J. R. Kumar and B. Banakara, "Finite Element Analysis in the Estimation of Air-Gap Torque and Surface Temperature of Induction Machine," *IOP Conference Series: Materials Science and Engineering*, vol. 225, p. 012116, 2017.
- [29] M. Popescu, N. Riviere, G. Volpe, M. Villani, G. Fabri, and L. Di Leonardo, "A Copper Rotor Induction Motor Solution for Electrical Vehicles Traction System," *2019 IEEE Energy Conversion Congress and Exposition, ECCE 2019*, pp. 3924–3930, 2019.